ADVANCES IN ATMOSPHERIC SCIENCES, VOL. 43, JANUARY 2026, 87–102

• **Original Paper** •

Impacts of 1.5°C and 2.0°C Global Warming on the Onset, Cessation, and Length of the Rainy Season in Global Land Monsoon Regions※

Thierry N. TAGUELA[1], Ibraheem RAJI[1], Akintomide A. AKINSANOLA[*1], Priyanshi SINGHAI[2], Oluwafemi E. ADEYERI[3], Caroline M. WAINWRIGHT[4], and Rondrotiana BARIMALALA[5]

[1]*Department of Earth and Environmental Sciences, University of Illinois Chicago, IL, USA*

[2]*School of Meteorology, University of Oklahoma, Norman, OK, USA*

[3]*ARC Centre of Excellence for the Weather of the 21st Century, Fenner School of Environment and Society, The Australian National University, Canberra, Australia*

[4]*University of Leeds, Leeds, UK*

[5]*NORCE, Bergen, Norway*

(Received 15 September 2024; revised 23 June 2025; accepted 2 July 2025)

ABSTRACT

The onset, cessation, and length of the rainy season are crucial for global water resources, agricultural practices, and food security. However, the response of precipitation seasonality to global warming remains uncertain. In this study, we analyze how global warming levels (GWLs) of 1.5°C and 2°C could affect the timing of rainfall onset (RODs), rainfall cessation (RCDs), and the overall duration of the rainy season (LRS) over global land monsoon (GLM) regions using simulations from CMIP6 under the SSP2-4.5 and SSP5-8.5 scenarios. With high model consensus, our results reveal that RODs are projected to occur later over Southern Africa, North Africa, and South America, but earlier over South Asia and Australia, in a warmer climate. The projected early RODs in Australia are more pronounced at the 2°C GWL under SSP5-8.5. On the other hand, early RCDs are projected over South America and East Asia, while late RCDs are projected over North Africa, with high inter-model agreement. These changes are associated with a future decrease in LRS in most GLM regions. Additionally, we found that continuous warming over 1.5°C will further reduce the length of the rainy season, especially over the South America, North Africa, and Southern Africa monsoon regions. The findings underscore the urgent need to mitigate global warming.

Key words: rainfall onset, rainfall cessation, global land monsoon, rainy season length, CMIP6 projections, global warming levels

Citation: Taguela, N. T., I. Raji, A. A. Akinsanola, P. Singhai, O. E. Adeyeri, C. M. Wainwright, and R. Barimalala, 2026: Impacts of 1.5°C and 2.0°C global warming on the onset, cessation, and length of the rainy season in global land monsoon regions. *Adv. Atmos. Sci.*, **43**(1), 87−102, https://doi.org/10.1007/s00376-025-4386-9.

Article Highlights:

- Future RODs over Southern Africa, North Africa, and South America will likely be delayed, while early RCDs are projected over South America.
- Changes in RODs and RCDs are associated with a future decrease in LRS in most GLM regions.
- Continuous warming over 1.5°C will further reduce the LRS, particularly in monsoonal South America, North Africa, and Southern Africa.

1. Introduction

The global land monsoon (GLM) system comprises seven major monsoon regions: North America (NAM), South America (SAM), North Africa (NAF), Southern Africa (SAF), South Asia (SAS), East Asia (EAS), and Australia (AUS) (Yim et al., 2014; Wang et al., 2017b; Wang et al., 2020). These regions are characterized by a seasonal reversal of wind direction driven by differential heating between land and ocean surfaces, leading to enhanced moisture transport and a pronounced increase in precipitation during the local summer season (Akinsanola and Zhou, 2019, 2020; Chen et al., 2020; Chakraborty and Singhai, 2021). The monsoon system plays a critical role in global hydrological and energy cycles, directly influencing the livelihoods,

※ This paper is a contribution to the special topic on Global and Regional Monsoons: State of the Art and Perspectives.

* Corresponding author: Akintomide A. AKINSANOLA
Email: aakinsan@uic.edu

water resources, and agricultural productivity of nearly two-thirds of the world's population (Wang and Ding, 2008; Wang et al., 2012; Kitoh et al., 2013; Zhang et al., 2016; Akinsanola and Zhou, 2019; Zhang and Zhou, 2020). However, these regions exhibit high sensitivity to global climate change, as warming-induced shifts in atmospheric circulation and moisture availability can alter monsoon intensity, duration, and variability (Seager et al., 2010; Kitoh et al., 2013; Zhang and Zhou, 2019; Zhou et al., 2020). Given the profound socioeconomic and ecological consequences of monsoon variability, robust and reliable projections of GLM precipitation characteristics are essential for improving climate adaptation and mitigation strategies in these vulnerable regions.

Over the past 30 years, the average global surface temperature has risen by about 0.2°C (10 yr)$^{-1}$ due to increased greenhouse gas concentrations, driven mainly by anthropogenic factors (IPCC, 2021). Studies have shown that this warming trend has a major impact on the hydrological cycle (Mishra and Liu, 2014; Lehmann et al., 2015; Donat et al., 2016), altering precipitation characteristics in GLM regions (Vera et al., 2006; Jones and Carvalho, 2013; Kitoh et al., 2013; Zhang et al., 2016; Akinsanola and Zhou, 2019, 2020; Deng et al., 2018; Ni and Hsu, 2018; Seth et al., 2019; Zhang and Zhou, 2019; Chen et al., 2020; Moon and Ha, 2020; Wang et al., 2020; Chang et al., 2022). For example, more frequent severe rainfall extremes have been documented in the AUS and SAM monsoon regions (Jones and Carvalho, 2013; Wang et al., 2020). Over SAS, precipitation shows decreased occurrence of low and moderate intensities triggering meteorological drought (Mishra and Liu, 2014), with an increasing positive trend in summer monsoon precipitation over the northern parts of India's west coast (Preethi et al., 2017). The summer monsoon rainfall in SAS has been consistently projected to rise (Kitoh et al., 2013; Menon et al., 2013; Sharmila et al., 2015), while in NAM, it will likely decrease (Jin et al., 2020). Regionally, because of the disparity in warming rates between hemispheres, projected changes in monsoon precipitation show a more significant and consistent increase in the Northern Hemisphere (NH) compared to the Southern Hemisphere (SH) (Lee and Wang, 2014). Earlier research has found that, under severe climate scenario pathways, there is a projected rise in the frequency of floods and droughts in eastern Africa (Ayugi et al., 2021). Future projections indicate a decrease in precipitation across both NAF and SAF, with NAF experiencing notably wet years and SAF facing significantly drier years by the end of the 21st century (Almazroui et al., 2020; Majdi et al., 2022; Bobde et al., 2024). Given these significant alterations in precipitation patterns, it is important to draw more attention to the timing of rainfall onset and cessation, along with the length of the rainy season to enhance our understanding and preparedness for the resulting hydrological impacts.

Although future GLM changes have received much attention, most studies have focused on understanding and predicting precipitation characteristics such as mean and extreme rainfall (e.g., Akinsanola and Zhou, 2019; Chen et al., 2020; Jin et al., 2020; Yao et al., 2021; Chang et al., 2022; Das et al., 2022; Liu et al., 2022), with limited attention to changes in onset and cessation dates of the rainy season. However, understanding the impact of global warming on these rainy season characteristics in GLM regions is vital for developing adaptive strategies in socioeconomic sectors such as agriculture, water resource management, and disaster preparedness (Turner and Annamalai, 2012). Early or delayed onset can significantly affect crop planting schedules and yields, while premature or prolonged cessation impacts water availability and increases the risk of droughts and floods (Gadgil and Gadgil, 2006; Dash et al., 2007; Sylla et al., 2016; Singhai et al., 2023). Findings from studies reveal that higher warming levels could trigger a delayed rainfall onset and early withdrawal due to variations in atmospheric circulation patterns and gradients of sea surface temperatures (SSTs) (Kitoh et al., 2013; Khadka et al., 2022). For instance, a projected average delay of 5–10 days in the start of the wet season in West Africa, along with a later onset in SAF, is linked to the intensifying Saharan heat low during late summer and a northward shift in the tropical rain belt from August to December (Dunning et al., 2018). Furthermore, Khadka et al. (2022) observed that most CMIP5 and CMIP6 models predict a late onset and early retreat for the Southeast Asian monsoon. However, under a high-emissions scenario, CMIP6 models project an earlier summer monsoon onset over the Arabian Sea and a delayed onset over the Bay of Bengal and South China Sea, driven by shifts in the northward migration of the equatorial intraseasonal oscillation (Wang et al., 2024). Moreover, Cheng et al. (2024) identified a significant correlation between delayed monsoon onset projections over the Bay of Bengal/South China Sea and western Pacific SST simulations, prompting adjustments that halved the projected delay. On the other hand, the projected duration of the Indian summer monsoon (ISM) shows reduced uncertainty when constrained by observed SST trends in the western Pacific and surface warming trends over the northern mid–high latitudes, suggesting a six-day reduction in ISM duration under a high-emissions scenario (Cheng et al., 2025). Additionally, based on observations and CMIP5 models, Hariadi et al. (2022) showed that the El Niño–Southern Oscillation (ENSO) influences the monsoon's onset and cessation dates in Southeast Asia, with El Niño events causing an early onset and La Niña events leading to a delayed onset. Similarly, more erratic onset and cessation patterns (Omondi et al., 2014), along with the duration of the rainy season (Sabeerali and Ajayamohan, 2018), are expected to be more pronounced toward the end of the 21st century.

Despite these significant advances in monsoon research, most studies have focused predominantly on individual regional monsoon systems, leaving a critical gap in our understanding of how rainy season characteristics respond to global warming at the broader GLM scale. Specifically, the response of key monsoon attributes—such as rainfall onset dates (RODs), cessation dates (RCDs), and the length

of the rainy season (LRS)—to future climate scenarios remains insufficiently explored across all GLM regions. Furthermore, limited research has systematically assessed how these characteristics evolve under different levels of global warming, particularly the 1.5°C and 2.0°C thresholds outlined in the Paris Agreement. Given the substantial societal and ecological dependence on monsoon rainfall, it is crucial to comprehensively evaluate the spatially heterogeneous impacts of climate change on monsoon dynamics. This study builds on previous studies to provide a comprehensive assessment of projected changes in RODs, RCDs, and LRS under varying warming scenarios across all GLM regions, offering critical insights for climate adaptation strategies and water resource management.

CMIP6 models are used to assess changes based on the Shared Socioeconomic Pathway (SSP) 2-4.5 and 5-8.5 scenarios. The rest of this paper is organized as follows: Section 2 details the data and methods employed in the study. Section 3 assesses how well the model simulates the climatology of onset dates, cessation dates, and length of the rainy season over GLM regions. Section 4 investigates projected changes in the onset, cessation, and duration of the rainy season, along with changes in key rainfall characteristics, including total rainfall, rainfall per rainy day, and the number of rainy days. Finally, section 5 presents a summary and conclusions.

2. Data and methods

This study uses historical and future precipitation datasets from 16 CMIP6 (phase 6 of the Coupled Model Intercomparison Project) models (Eyring et al., 2016), as detailed in Table S1 in the electronic supplementary material (ESM). These datasets encompass the historical period (1995–2014) as defined in IPCC AR6, and the future (2015–2100). The study employs the SSP2-4.5 and SSP5-8.5 scenarios, reflecting moderate mitigation and worst-case scenarios. Moderate mitigation efforts are anticipated in the SSP2-4.5 scenario, potentially limiting global warming to approximately 2.5°C above pre-industrial levels by the end of the 21st century (O'Neill et al., 2017). Conversely, the SSP5-8.5 scenario, also known as "business as usual," depicts a future with high fossil fuel use and limited efforts in climate mitigation, resulting in an approximate 5°C increase in temperature by the close of the 21st century. The first realization (r1i1p1f1) is used in each model's historical and future projections to maintain consistency in the analysis. The study also explores the warming thresholds of 1.5°C and 2.0°C compared to pre-industrial levels. These thresholds are identified as the initial year when the 21-year running mean of the global mean surface temperature (GMST) arrives at 1.5°C and 2.0°C above pre-industrial levels. Two 10-year periods around each threshold are selected (Ayugi et al., 2022; Hauser et al., 2022). Table 1 presents the timing of reaching 1.5°C and 2.0°C of global warming relative to pre-industrial levels under the SSP2-4.5 and SSP5-8.5 scenarios. The CMIP6 multimodel ensemble mean approach (referred to here as "EnsMean") is employed to address systematic biases due to model differences (Akinsanola and Zhou, 2019). The historical performance of the CMIP6 models, along with their EnsMean, is evaluated using observed daily datasets from the unified gauge-based analysis of global daily precipitation (CPC) at 0.5° × 0.5° resolution (Xie et al., 2010). In addition, we use CPC data to identify the land areas of the global monsoon (GM) domain. Following Wang et al. (2012) and Chen et al. (2020), we defined the GM domain as the area where the precipitation difference between local summer and winter

Table 1. Timing of each CMIP6 model for reaching 1.5°C and 2.0°C global warming levels (GWLs) under the SSP2-4.5 and SSP5-8.5 scenarios (Hauser et al., 2022).

	SSP2-4.5		SSP5-8.5	
Model name	GWL 1.5°C	GWL 2.0°C	GWL 1.5°C	GWL 2.0°C
ACCESS-CM2	2019–38	2031–50	2016–35	2029–48
ACCESS-ESM1-5	2020–39	2036–55	2018–37	2030–49
CanESM5	2004–23	2015–34	2003–22	2013–32
CESM2-WACCM	2015–34	2030–49	2011–30	2024–43
CMCC-CM2-SR5	2016–35	2029–48	2012–31	2024–43
CMCC-ESM2	2021–40	2031–50	2020–39	2030–49
EC-Earth3	2013–32	2035–54	2015–34	2026–45
INM-CM4-8	2026–45	2054–73	2021–40	2037–56
INM-CM5-0	2028–47	2063–82	2021–40	2037–56
IPSL-CM6A-LR	2009–28	2024–43	2009–28	2025–44
MIROC6	2037–56	2064–83	2031–50	2044–63
MPI-ESM1-2-HR	2028–47	2054–73	2024–43	2040–59
MPI-ESM1-2-LR	2027–46	2048–67	2025–44	2039–58
MRI-ESM2-0	2021–40	2040–59	2017–36	2029–48
NESM3	2015–34	2033–52	2011–30	2024–43
TaiESM1	2022–41	2034–53	2019–38	2027–46

exceeds 2.0 mm d^{-1}, and local summer precipitation accounts for more than 55% of the annual total precipitation. Summer here refers to May to September for the NH and November to March for the SH.

To compare all datasets, we remap them using first-order conservative remapping onto a common spatial grid of 2.81° × 2.81°, adhering to the lowest model resolution following Faye and Akinsanola (2022) and Akinsanola et al. (2024, 2025). Next, the metrics (e.g., onset date) are calculated for each model and averaged to obtain the EnsMean of the models. Assessing model performance in simulating historical precipitation is crucial for identifying uncertainty sources and enhancing confidence in future projections. Here, CMIP6 models are evaluated against observations using the percentage bias (%) [Eq. (1)], normalized root-mean-square error [NRMSE: Eq. (2)], pattern correlation coefficient [PCC: Eq. (3)], and Taylor skill score [TSS: Eq. (4)]. Results are summarized through portrait diagrams, providing a clear comparison of model performance across all monsoon regions (Akinsanola et al., 2021; Taguela et al., 2025).

$$\%\text{BIAS} = \frac{\sum_{i=1}^{n}(M_i - O_i)}{\sum_{i=1}^{n} O_i} \times 100\,, \tag{1}$$

$$\text{NRMSE} = \frac{\sqrt{\frac{1}{n}\sum_{i=1}^{n}(M_i - O_i)^2}}{\frac{1}{n}\sum_{i=1}^{n} O_i}\,, \tag{2}$$

$$\text{PCC}(M,O) = \frac{\text{cov}(M,O)}{\sqrt{\text{Var}(M) \times \text{Var}(O)}}\,, \tag{3}$$

$$\text{TSS} = \frac{4(1+\text{PCC})^2}{\left(\frac{\sigma M}{\sigma O} + \frac{\sigma O}{\sigma M}\right)^2 (1+\text{PCC}_0)^2}\,, \tag{4}$$

where O and M are the observation and reference model means, respectively; "cov" stands for covariance while "var" is variance; and n is the total number of time steps. The standard deviation is denoted by σ, while PCC_0 represents the highest possible value of PCC, set to 1. The TSS varies between 0 and 1, indicating no match or a perfect match between the model and the observations. Numerous studies have employed the TSS to evaluate model performance (e.g., Faye and Akinsanola, 2022; Bobde et al., 2024).

The onset and cessation dates are determined using the approach outlined by Liebmann and Marengo (2001), with adjustments introduced by Bombardi et al. (2019). The method uses only precipitation data and has been applied across the global monsoon region by Wainwright et al. (2021) and Bombardi and Boos (2021). The daily accumulation of precipitation anomalies (S), beginning from the dry season, is used to detect onset and cessation dates. Based on the region's climatology, S defines a threshold that accounts for the persistence of precipitation leading up to these dates. The onset date is identified when S reaches a local minimum, while the cessation date is determined retrospectively by applying the same calculation from the year's end backward. S is calculated using Eq. (5) as follows:

$$S = \sum_{i=t_0}\left(P_i - \overline{P}\right)\,, \tag{5}$$

where P_i represents the amount of precipitation measured daily on day i; $\overline{P}$ denotes the mean annual precipitation rate over a long term, measured in mm d^{-1}; and t_0 marks the beginning date for the computations. It should be noted that this method does not consider areas with two or three wet seasons annually. This is achieved by analyzing the proportion of variance explained by the initial three harmonics of the mean annual precipitation cycle. If the second or third harmonic accounts for as much variance as the first harmonic or more, it suggests a pronounced bimodal or trimodal precipitation regime, leading to the region being masked (Bombardi et al., 2019). The duration of the rainy season is defined as the period between the start and end dates of rainfall. We also assess potential future changes in the frequency and intensity of rainfall during the season, defining a rainy day as having more than 1 mm of precipitation, in line with the criteria used in CLIMDEX indices (Zhang et al., 2011). The average precipitation during these wet days is then computed to represent the intensity of heavy rainfall (Dunning et al. 2018).

The projected changes are determined by comparing the 20-year time slice from the projection (see Table 1 for the period) with the historical period (1995–2014), and future changes are deemed robust when a minimum of 70% of individual models align on the direction or sign of the ensemble mean. To evaluate the possibility of mitigating the effects of reaching 2.0°C above pre-industrial levels, the avoided impacts caused by an extra 0.5°C increase in warming are calculated using Eq. (6), and expressed as percentages (%):

$$\text{Avoided Impacts} = \left(\frac{\text{GW}_{2.0} - \text{GW}_{1.5}}{\text{GW}_{2.0}}\right) \times 100\,. \tag{6}$$

$\text{GW}_{1.5}$ and $\text{GW}_{2.0}$ represent the changes associated with 1.5°C and 2.0°C warming compared to the historical period. This method has been employed in several recent studies (e.g., Chen et al., 2020; Wang et al., 2020; Ayugi et al., 2022).

3. Mean climatology of onset, cessation, and length of the rainy season

We begin by evaluating the capability of CMIP6 models to reproduce the climatological mean of RODs, RCDs, and LRS across GLM regions by comparing model outputs with CPC observations (Fig. 1). Observations indicate that RODs typically occur during boreal (austral) spring, whereas RCDs generally take place during boreal (austral) fall (Figs. 1a and d) in the NH (SH). This seasonal pattern is driven primarily by the latitudinal migration of the Intertropi-

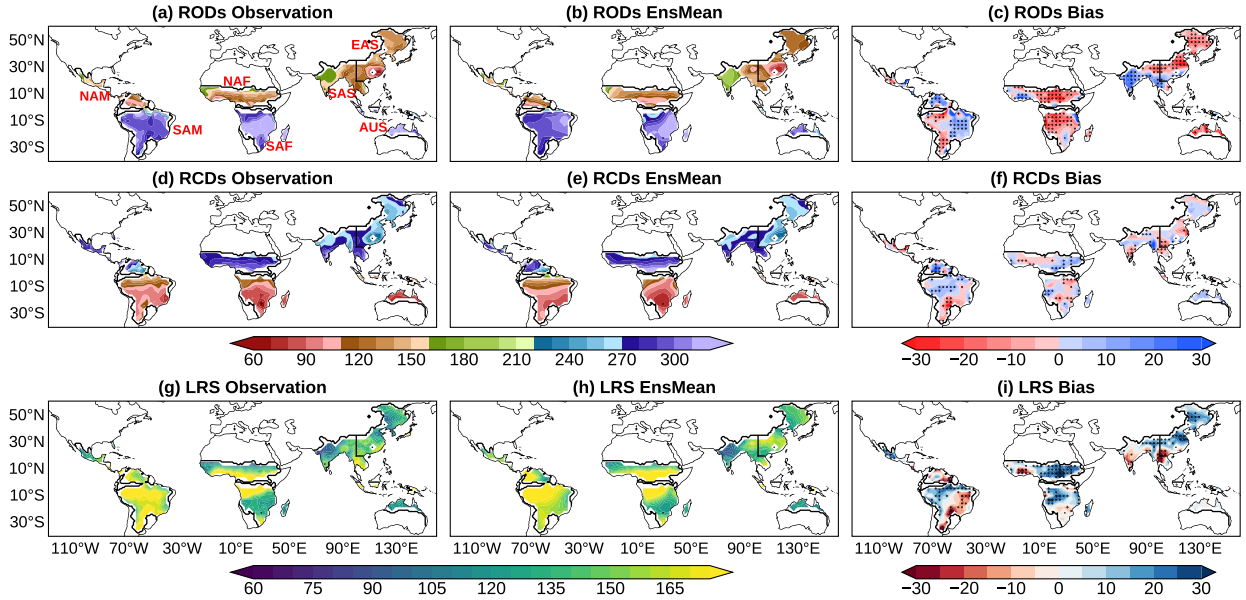

Fig. 1. The climatological mean (1995–2014) for (a–c) rainfall onset dates (RODs), (d–f) rainfall cessation dates (RCDs), and (g–i) length of the rainy season (LRS), measured in Julian days. The figures represent (a, d, g) observational data, (b, e, h) the CMIP6 EnsMean, and (c, f, i) biases of EnsMean relative to observations (measured in days). Areas with stippling in (c, f, i) are regions where differences are statistically significant at the 95% confidence level according to Student's *t*-test. The black contour lines outline the GLM domains, including North America (NAM), North Africa (NAF), South America (SAM), Southern Africa (SAF), East Asia (EAS), South Asia (SAS), and Australia (AUS).

cal Convergence Zone (ITCZ), which modulates convection throughout the year (Nicholson, 2018; Daron et al., 2019). However, mesoscale circulations, orographic influences, and land-use changes also contribute to regional variations in the timing of rainfall onset and cessation (Mugalavai et al., 2008; Amekudzi et al., 2015; Atiah et al., 2021; Omay et al., 2023; Mwangi et al., 2024). While some monsoonal regions exhibit significant spatial variability in RODs and RCDs, others display more consistent seasonal characteristics. For example, in the NAF monsoon region, RODs exhibit a zonally consistent northward progression, beginning along the coast in late March (Julian Day ~90) and reaching ~18°N by mid-June (Julian Day ~170) (Fig. 1a). This pattern aligns with that found by Kumi and Abiodun (2018), who analyzed the historical RODs, RCDs, and LRS over West Africa using CHIRPS (Hazard Group Infrared Precipitation with Stations) and ARC2 (African Rainfall Climatology version 2) observations. Although moisture transport in this region also originates from the Mediterranean and the Indian Ocean (Adeyeri et al., 2024), the northward progression of RODs is driven primarily by the northward transport of moisture by the West African Monsoon, which advects moisture from the Gulf of Guinea into the subcontinent (Omotosho et al., 2000; Sylla et al., 2013; Akinsanola and Zhou, 2020). In contrast, the spatial distribution of RODs and RCDs is more homogeneous across NAM and EAS (Figs. 1a and d), except in the southeastern part of EAS, where RODs occur significantly earlier than in other parts of the region (Fig. 1a).

EnsMean generally captures the key spatial climatology of RODs (Fig. 1b) and RCDs (Fig. 1e) across GLM regions. However, compared to observations, EnsMean exhibits a systematic delay in RODs of approximately 20–30 days over SAS and 10–20 days over eastern SAM and northern NAM, while advancing RODs by 20–30 days over NAF and EAS (Fig. 1c). In contrast, the simulated RCDs show lower biases than the RODs (Fig. 1f), with an advance of about 10–15 days over NAF and NAM and a delay of approximately 10 days over AUS.

Regarding LRS, observations indicate that among the monsoon regions, SAM experiences the longest LRS (> 160 days), while SAS has the shortest (< 90 days) (Fig. 1g). This spatial pattern is relatively well captured by EnsMean (Fig. 1h), though biases in duration remain (Fig. 1i). Specifically, EnsMean overestimates LRS by up to 30 days over eastern NAF, primarily due to earlier RODs (Fig. 1c). Additionally, a positive bias of about 15 days is observed over EAS, while SAS exhibits a negative bias of approximately 10 days. A distinct dipole bias emerges in the SAM region, with LRS overestimated by roughly 20 days in the western part and underestimated by a similar margin in the eastern part.

Additionally, we evaluate the performance of individual models in reproducing the mean climatology of RODs, RCDs, and LRS across each monsoon region, and the results are presented using portrait diagrams illustrating the percentage bias, NRMSE, PCC, and TSS. These metrics measure the differences between the climatological mean of the observations and models (Fig. 2). Previous studies have demonstrated the effectiveness of these diagrams (e.g., Taguela et al., 2020; Akinsanola et al., 2021; Bobde et al., 2024). A desirable outcome is to have a low percentage bias

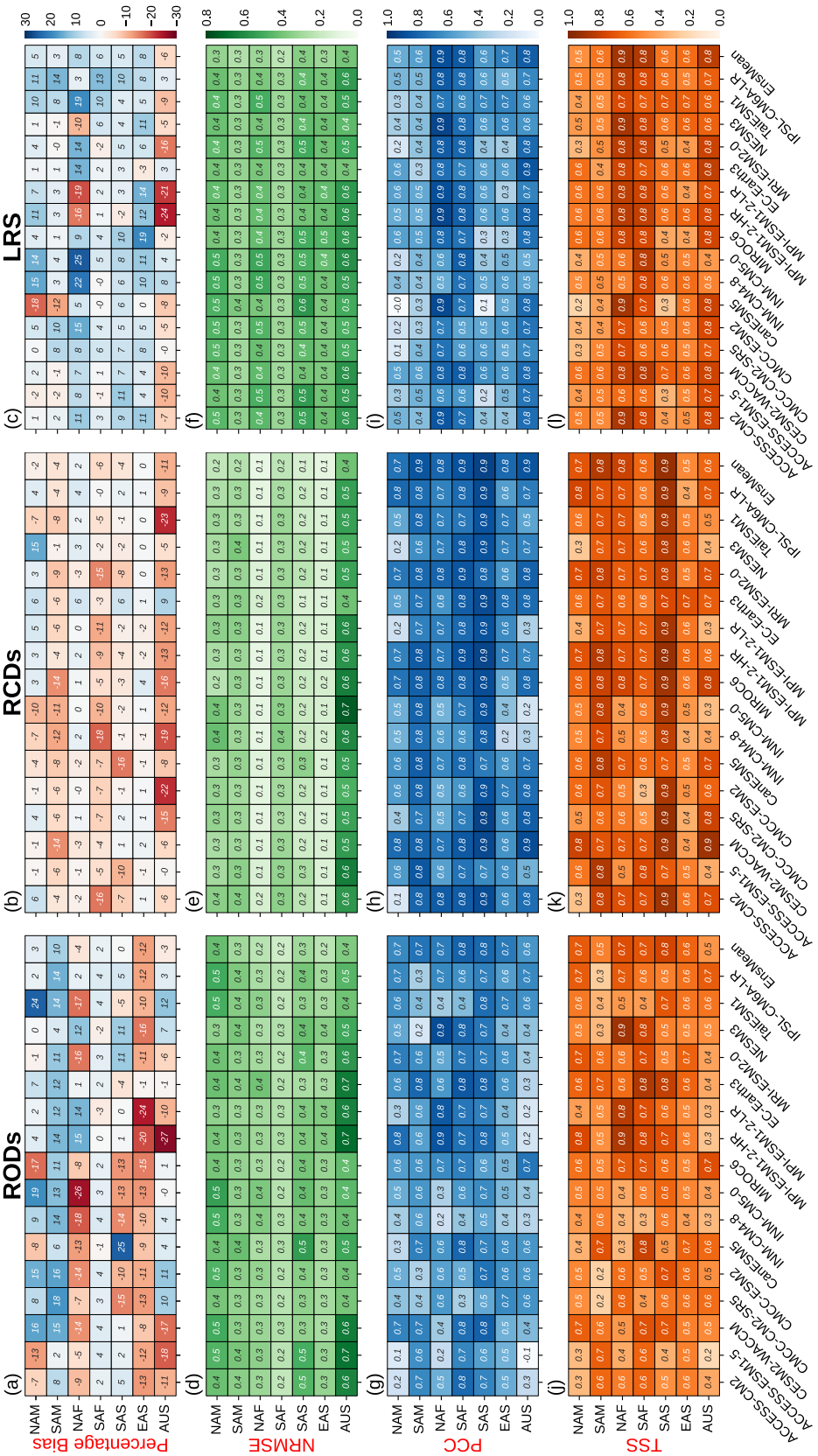

Fig. 2. Portrait diagrams showing the (a–c) percentage bias (units: d), (d–f) normalized root-mean-square error (NRMSE), (g–i) pattern correlation coefficient (PCC; %), and (j–l) Taylor skill score (TSS) of the (a, d, g, j) rainfall onset dates (RODs), (b, e, h, k) rainfall cessation dates (RCD), and (c, f, i, l) rainy season length (LRS) in each GLM region for individual models, along with the CMIP6 EnsMean compared with CPC during the period 1995–2014.

and NRMSE, along with high values for PCC and TSS (Akinsanola et al., 2024; Bobde et al., 2024). Figure 2 shows that, across the GLM regions, CMIP6 models have difficulty simulating RODs (Fig. 2a) compared to RCDs (Fig. 2b). This is indicated by the higher percentage bias values for RODs relative to RCDs, with values as large as −26% in the NAF region for models such as INM-CM5-0 (Fig. 2a), leading to a high LRS percentage bias of 25% (Fig. 2c). The models' NRMSE values (Figs. 2d–f) are relatively low across most monsoon regions, except over AUS, where the NRMSE values for RODs, RCDs, and LRS are higher, with most models showing values between 0.5 and 0.7. Positive PCC values are generally observed (Figs. 2g–i), with most models reaching up to 0.8–0.9 in SAS for RODs and RCDs, and in NAF and AUS for LRS. The TSS for RODs, RCDs, and LRS indicates regional variations across models (Figs. 2j–l). AUS exhibits the lowest scores for RODs (Fig. 2j) and the highest for LRS (Fig. 2l), while SAS shows the highest scores for RCDs, reaching 0.9 for most models (Fig. 2k). Overall, while some individual models display significant biases, EnsMean consistently outperforms most individual models across all variables (RODs, RCDs, and LRS) and evaluation metrics (percentage bias, NRMSE, PCC, and TSS). This highlights EnsMean as a more reliable choice for further analysis and discussion over GLM regions.

4. Changes in rainy season characteristics

4.1. *Projected changes in the onset, cessation, and length of the rainy season*

The projected changes in RODs, RCDs, and LRS over GLM regions under the SSP2-4.5 and SSP5-8.5 scenarios are shown in Fig. 3 for different GWLs. Earlier RODs are projected over EAS (about 4 days earlier at 2.0°C under the SSP2-4.5 scenario). Projected RODs in EAS align with results from Ha et al. (2020). However, across most GLM regions, regardless of scenario or warming level (Figs. 3a, d, g, j), EnsMean generally projects a delay in future RODs. This agrees with findings from Dwyer et al. (2014), Dunning et al. (2018), and Wainwright et al. (2021). The delays in future RODs could be attributable to reduced latent heat fluxes linked to negative soil moisture anomalies (Collini et al., 2008). These delays increase with continuous warming, reaching 4–5 days under SSP2-4.5 and 6–7 days under SSP5-8.5 in NAF, SAF, and SAM at the 2.0°C GWL (Fig. 3j). The projected delay in RODs is particularly robust over SAM and SAF, with at least 70% of the models agreeing on the sign of the change in EnsMean across these regions. Additionally, models show relatively low uncertainty in the projected changes in RODs across SAM, with spreads ranging from −1 to 5 days under the 2°C warming level for both scenarios (Figs. 4b and 5b, and Fig. S3b in the ESM). The highest uncertainties in the projected RODs (±15 days) are observed over AUS (Fig. S3g in the ESM), where EnsMean projects advanced RODs under both scenarios (Figs. 3a, d, g and j). This advancement is more pronounced under 2.0°C global warming, reaching up to 10 days under the SSP5-8.5 scenario (Fig. 3j). For projected changes in RCDs (Figs. 3b, e, h and k), delays (advancements) are observed under all scenarios and warming levels over NAF (SAM), reaching 5 to 6 (4 to 5) days under SSP5-8.5 at the 2.0°C warming level (Fig. 3k). These delays in RCDs are robust over NAF, with

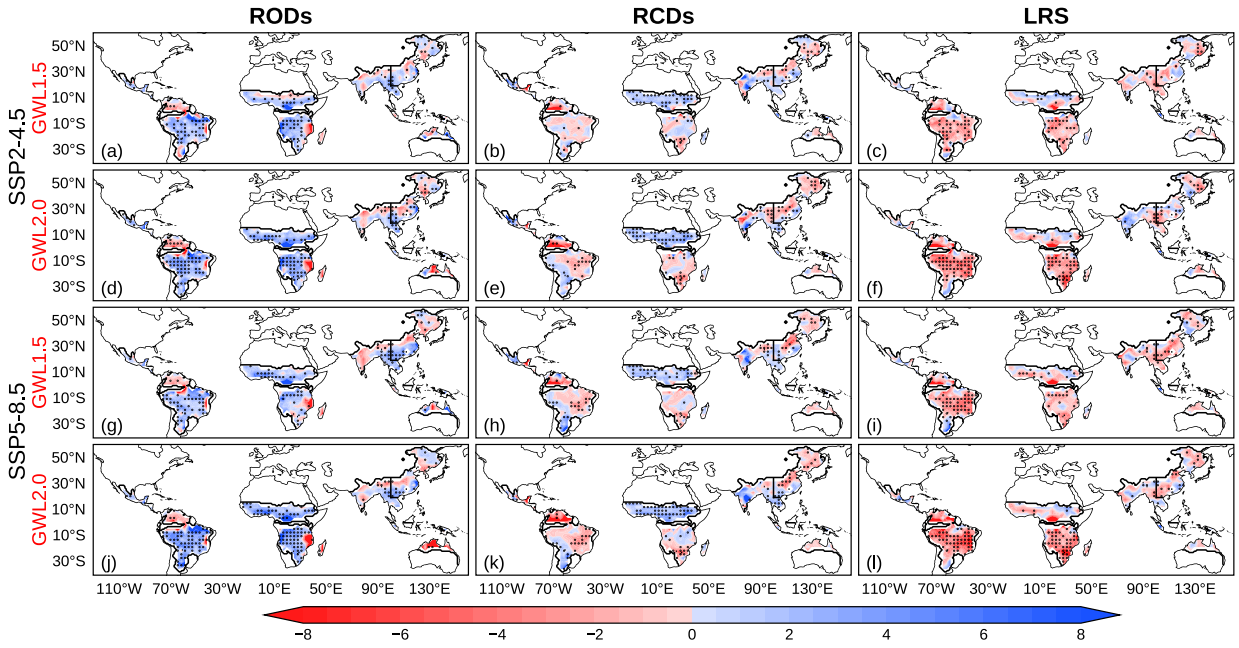

Fig. 3. Future changes in rainfall onset dates (RODs), rainfall cessation dates (RCDs), and length of the rainy season (LRS) across GLM regions, compared to the period 1995–2014 based on the CMIP6 EnsMean under the SSP2-4.5 and SSP5-8.5 scenarios at various GWLs: (a–c) SSP2-4.5/1.5°C; (d–f) SSP2-4.5/2.0°C; (g–i) SSP5-8.5/1.5°C; and (j–l) SSP5–8.5/2.0°C. Stippling marks areas where at least 70% of the models concur on the direction of change in EnsMean.

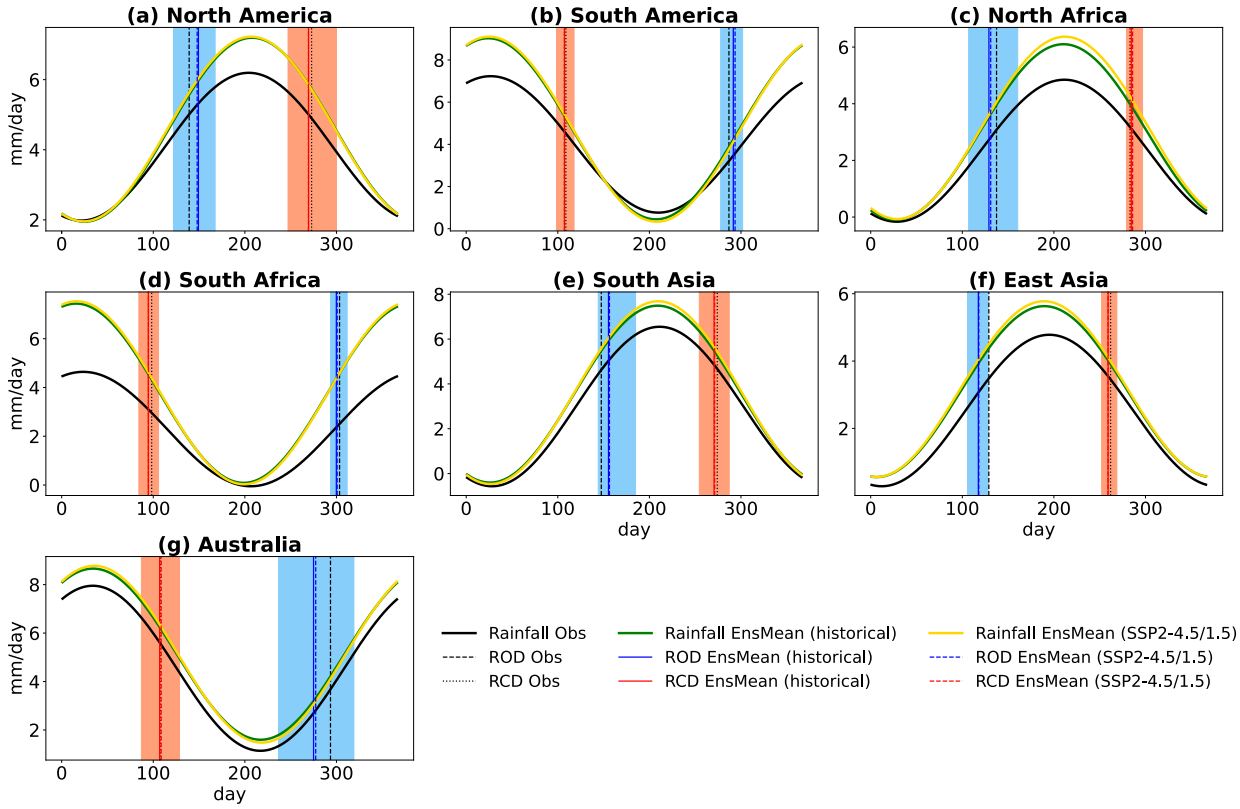

Fig. 4. Annual rainfall cycle from observations (1995–2014, CPC: black line), CMIP6 EnsMean for the historical period (1995–2014: green line), and future projections under SSP2-4.5 at the 1.5°C GWL (yellow line). Vertical dashed and dotted black lines indicate observed rainfall onset and cessation dates, while solid blue and red lines represent the CMIP6 historical EnsMean for these dates. Projected onset and cessation dates are shown with dashed blue and red lines, respectively, with light shading in corresponding colors representing model spread. The annual cycles are smoothed representations of the long-term daily means, derived using the first harmonic of Fourier analysis.

strong model consensus. All scenarios also project an advancement of approximately 5 days (2 days) over NAM (AUS). However, the highest uncertainties in projected RCDs are found over NAM, with model spreads between −10 and 10 days (Figs. 4a and 5a, and Figs. S1a–S3a in the ESM), while the lowest uncertainties are over EAS, with spreads between −3 and 3 days (Figs. 4f and 5f, and Figs. S1f–S3f in the ESM).

Under the combined impacts of changes in RODs and RCDs, LRS is expected to decrease over SAM and SAF under both the SSP2-4.5 and SSP5-8.5 scenarios (Figs. 3c, f, i and l), with a pronounced decrease (> 8 days) under 2.0°C global warming in each scenario. This is likely related to the projected delays in RODs in these regions (Figs. 3a, d, g and j). Although the shortening in LRS over SAF shows strong model consensus only under 2.0°C warming in each scenario (Figs. 3f and l), the decrease over SAM is robust under both 1.5°C and 2.0°C warming in both scenarios. Although some studies suggest a rise in LRS of the East Asian monsoon (Kitoh et al., 2013; Lee and Wang, 2014; Moon and Ha, 2020), consistent with Sabeerali and Ajayamohan (2018) and except at 2°C under SSP2-4.5, a projected decrease in LRS is also observed over SAS and EAS. Sabeerali and Ajayamohan (2018) attributed this decrease primarily to the warming of the western Indian Ocean, which reduces the upper-tropospheric temperature gradient and consequently reduces the LRS. Uncertainties in the projected LRS are highest over EAS (Fig. S3c in the ESM) and lowest over AUS (Fig. S3g in the ESM).

Figures S4 in the ESM and 6 explore the effect of an additional 0.5°C global warming climate on RODs, RCDs, and LRS over GLM regions under the Paris Agreement's proposed warming level of 1.5°C (COP21, 2015). The additional effects resulting from 2.0°C warming lead to further delay in RODs over NAF, SAF, SAS, and SAM, while earlier RODs are projected over AUS (Figs. S4a and d in the ESM). Over NAF (SAM), the delay is more substantial under SSP2-4.5 (SSP5-8.5) compared to SSP5-8.5 (SSP2-4.5). However, limiting the warming to below 1.5°C rather than 2.0°C will lead to positive avoided impacts on RODs in most GLM regions, such as SAS (18%) and SAM (41%) under the SSP2-4.5 and SSP5-8.5 scenarios, respectively (Figs. 6a and b). In contrast, the increase in warming from 1.5°C to 2.0°C further advances RODs by more than 6 days over AUS under the SSP5-8.5 scenario (Fig. S4d in the ESM). For the projected RCDs under SSP2-4.5, additional warming above 1.5°C causes a slight delay of about 2 days over NAF, while a more pronounced delay of about 4 days

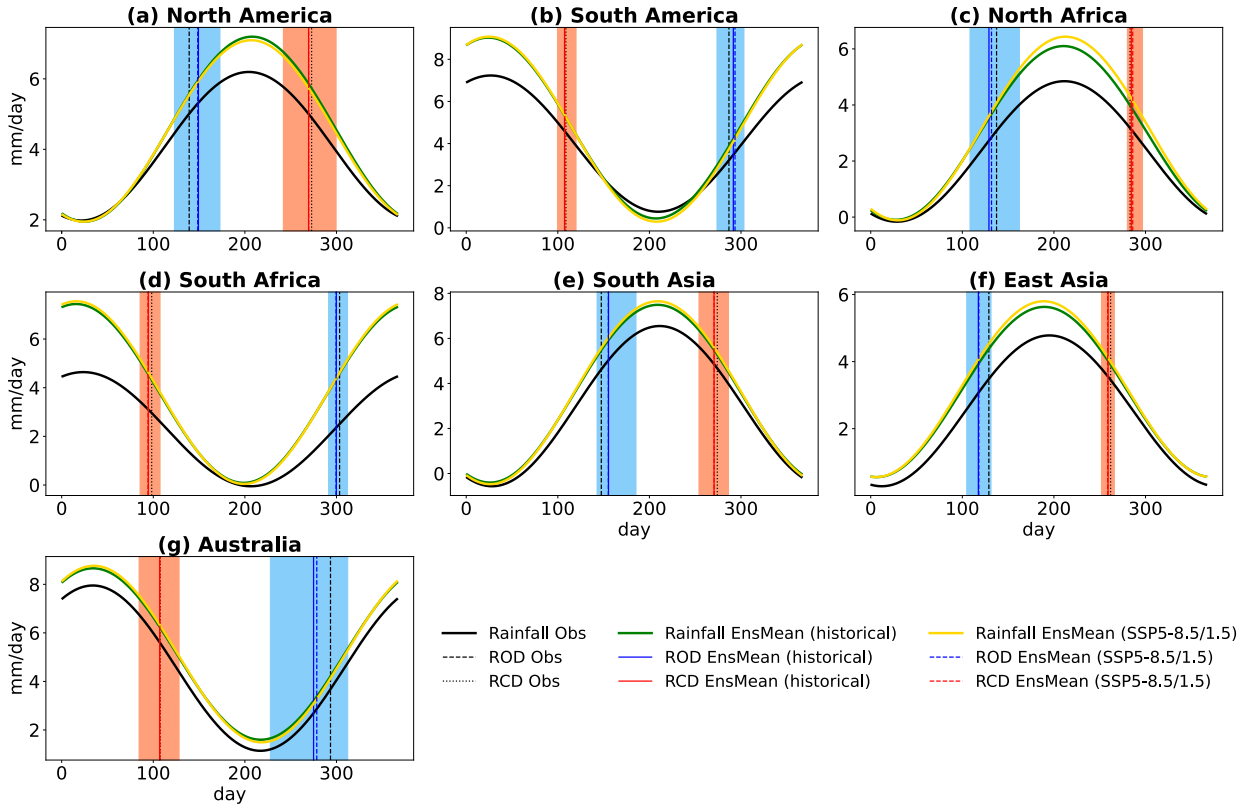

Fig. 5. Annual rainfall cycle from observations (1995–2014, CPC: black line), the CMIP6 EnsMean for the historical period (1995–2014: green line), and future projections under SSP5-8.5 at the 1.5°C GWL (yellow line). Vertical dashed and dotted black lines indicate observed rainfall onset and cessation dates, while solid blue and red lines represent the CMIP6 historical EnsMean for these dates. Projected onset and cessation dates are shown with dashed blue and red lines, respectively, with light shading in corresponding colors representing the model spread. The annual cycles are smoothed representations of the long-term daily means, derived using the first harmonic of Fourier analysis.

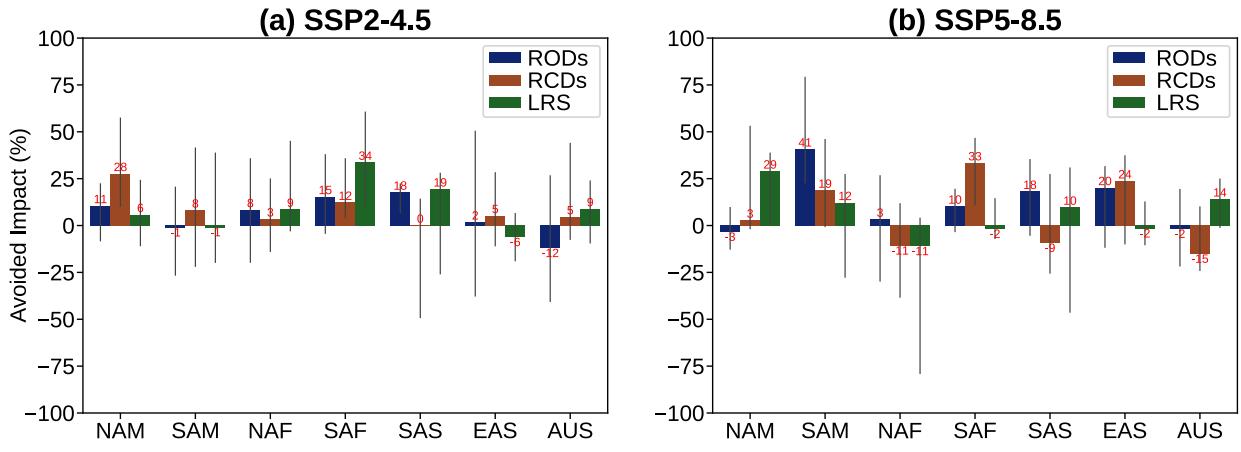

Fig. 6. Avoided impact of a 0.5°C warmer climate relative to the 1.5°C warming target over GLM regions (%) for rainfall onset dates (RODs), rainfall cessation dates (RCDs), and length of the rainy season (LRS) based on the CMIP6 EnsMean under the (a) SSP2-4.5 and (b) SSP5-8.5 scenarios. Projected changes are computed relative to the 1995–2014 historical period, and the error bars (vertical lines) represent the 95% confidence interval based on the spread across all CMIP6 models.

is projected under SSP5-8.5 (Figa. S4b and e in the ESM). The effect of an additional 0.5°C global warming will advance (delay) RCDs by approximately 6 days (5 days) over the western part of SAS under SSP2-4.5 (SSP5-8.5) (Figs. S4c and f in the ESM). Under a warmer climate, LRS is projected to be longer by about 5 days over SAS for SSP2-4.5 compared to SSP5-8.5. In both scenarios, a further decrease in LRS is projected over SAM and SAF with model consensus, and the shortest LRS is expected under the SSP5-8.5 scenario (Figs. S4c and f in the ESM). Limiting

the warming to below 1.5°C rather than 2.0°C will avoid 34% of the impact on the projected LRS in SAF under SSP2-4.5 (Figs. 6a and b). These findings suggest that a warming climate leads to a reduced likelihood of LRS, which could result in dry conditions over regions such as SAM and SAF.

4.2. *Future changes in precipitation characteristics within the rainy season*

This section investigates how precipitation characteristics during the rainy season will be affected by 1.5°C and 2.0°C increases in global temperatures under the SSP2-4.5 and SSP5-8.5 scenarios across GLM regions. Results show a projected increase in total precipitation over WAF, SAS, and EAS (Figs. 7a, d, g and j), with the increase stronger under the 2.0°C GWL in both scenarios (Figs. 7d and j) and higher increases (> 80 mm) over NAF (Figs. 7j and 8a). The projected increase in precipitation over NAF agrees with findings from Almazroui et al. (2020) and Dosio et al. (2021). The model consensus observed over NAF in both scenarios and at both GWLs (Figs. 7a, d, g and j) further indicates the robustness of the change in that region. The projected rise in precipitation could be linked to greater surface evaporation and intensified convergence of atmospheric moisture, as reported by Akinsanola and Zhou (2019). Conversely, although less robust, a projected decrease in total precipitation is observed over SAM, as also highlighted by Hodnebrog et al. (2022) and Almazroui et al. (2021). The decrease reaches −30 mm under SSP5-8.5 (Figs. 7g and j). For both GWLs, total precipitation is projected to increase under SSP2-4.5 and decrease under SSP5-8.5 in NAM (Figs. 7a, d, g, j, and 8a). However, that region has large model uncertainties at the 2.0°C GWL under the SSP5-8.5 scenario (Fig. 8a). For the projected amount of rainfall per day, an increase is expected in all regions (Figs. 7b, e, h and k). The projected increase is stronger at the 2.0°C GWL in both scenarios, with the highest (> 0.6 mm d^{-1}) and more robust increase projected over NAF under SSP5-8.5 (Fig. 7k). Conversely, the projected number of rainy days is expected to decrease in most monsoon regions (Figs. 7c, f, i and l). The highest decrease is expected over SAM and SAF and is more pronounced (> 10 days) at the 2.0°C GWL in both scenarios (Figs. 7f and l), with high model consensus. However, large uncertainties exist over SAM at the 2.0°C GWL under the SSP5-8.5 scenario (Fig. 8c). Notably, NAF exhibits the highest increase in the projected number of rainy days, reaching up to 8 days under the SSP5-8.5 scenario at the 2.0°C GWL.

Figure 9 explores the relationship between changes in total rainy season rainfall (TRSR) and changes in RODs as well as RCDs. While results vary across regions, the correlation between TRSR and RCDs is generally stronger. In SAF, under SSP2-4.5 at 1.5°C, the correlation between TRSR and RCDs reaches 0.59. Figure S5 in the ESM also illustrates the statistical relationships between TRSR and the rainfall per rainy day (RPRD), as well as the relationships between TRSR and the number of rainy days (NORD) across the 16 CMIP6 models. TRSR generally exhibits a stronger correlation with RPRD across all regions at both GWLs and under both scenarios, with the highest correlation coefficients observed in EAS, reaching up to 0.95 at a the

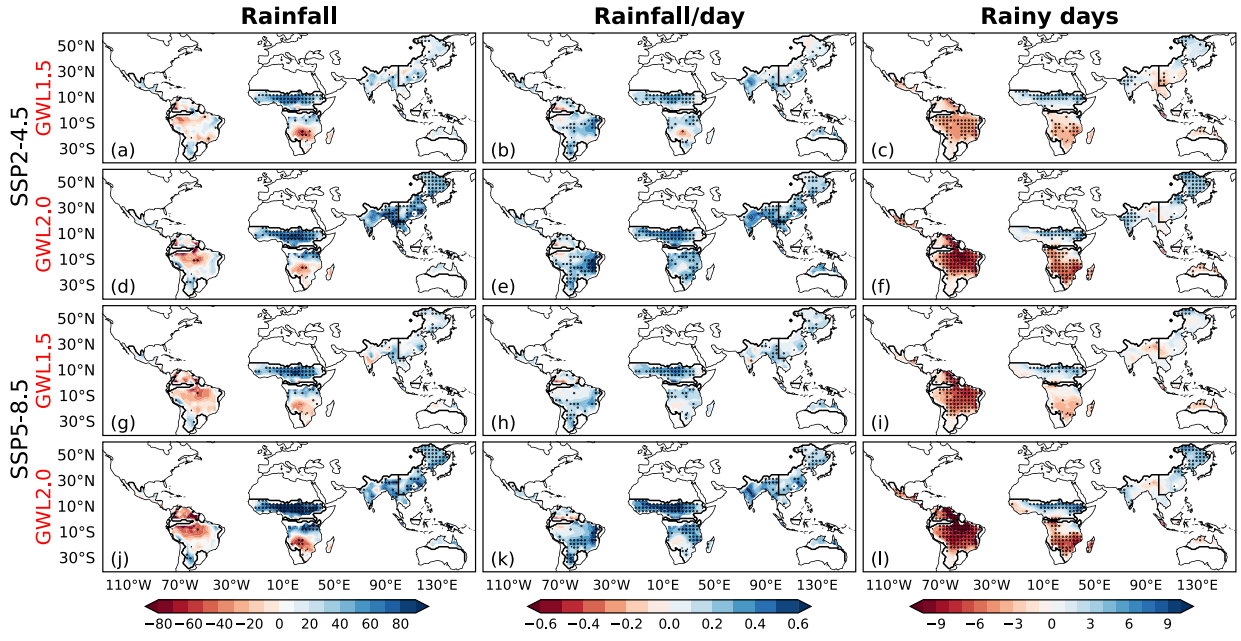

Fig. 7. Future changes in total rainfall during the rainy season (units: mm), daily rainfall amounts (units: mm d^{-1}), and number of rainy days (units: d) across GLM regions relative to the period 1995–2014 for the CMIP6 EnsMean under the SSP2-4.5 and SSP5-8.5 scenarios at different GWLs: (a–c) SSP2-4.5 under 1.5°C; (d–f) SSP2-4.5 under 2.0°C; (g–i) SSP5-8.5 under 1.5°C; and (j–l) SSP5-8.5 under 2.0°C. Stippling marks areas where at least 70% of the models concur on the direction of change in EnsMean.

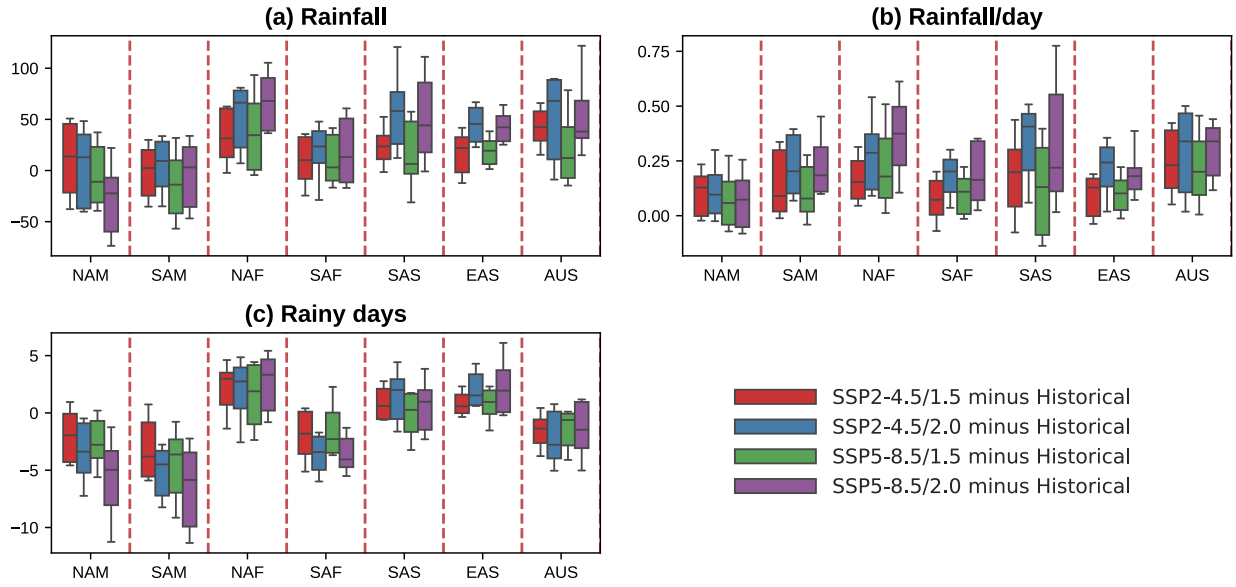

Fig. 8. Projected changes in the area-averaged (a) total rainfall during the rainy season (units: mm), (b) daily rainfall amount (units: mm d^{-1}), and (c) number of rainy days (units: d) under the SSP2-4.5 and SSP5-8.5 scenarios at various GWLs compared to the period 1995–2014 across different monsoon regions. Box-and-whisker plots illustrate the 10th, 25th, 50th, 75th, and 90th percentiles.

1.5°C GWL under the SSP2-4.5 scenario (Fig. S5 in the ESM). This suggests that, in many regions, the rise in RPRD might have a greater impact on TRSR than the changes in NORD. This aligns with the findings of Piao et al. (2023) over EAS, who reported a high correlation between TRSR and the rainfall per rainy season. However, TRSR is also closely associated with the NORD over SAS, with correlation coefficient values of 0.75 at the 2.0°C GWL under SSP2-4.5, and 0.75 at the 1.5°C GWL under SSP5-8.5 (Fig. S5 in the ESM).

From the 1.5°C to 2.0°C GWL, under both scenarios, there is a significant rise in TRSR and RPRD across most areas (Fig. 10 and Fig. S6 in the ESM). Over NAF (SAS), TRSR increases by more than 30 mm under SSP5-8.5 (SSP2-4.5), while the increase is less significant under SSP2-4.5 (SSP5-8.5) (Figs. 10a and d). For corresponding changes in RPRD, the increase is also more significant under the SSP5-8.5 scenario in most regions, with the largest increase (> 0.4 mm d^{-1}) observed west of the SAS region (Figs. 10b and e). However, for both TRSR and RPRD, the impact of 2.0°C over 1.5°C generally shows larger uncertainties under the SSP5-8.5 scenario (Figs. S6a and b in the ESM). With additional warming of 0.5°C, NORD decreases in all regions except SAS and EAS under the SSP2-4.5 scenario (Figs. 10c and f). The highest decrease of about 5 days is observed over SAM. Conversely, NAF and AUS exhibit an increase in NORD under the SSP5-8.5 scenario.

5. Summary and conclusion

Exceeding the 1.5°C and 2.0°C global warming thresholds is projected to induce profound changes in GM systems, with potentially devastating consequences for billions of people. This study addresses the critical question of how GLM rainfall patterns such as RODs, RCDs, and LRS will change in the future by analyzing historical and projected precipitation data from 16 CMIP6 models under the SSP2-4.5 and SSP5-8.5 scenarios.

Our results indicate that the CMIP6 EnsMean generally captures the basic spatial features of RODs and RCDs, albeit with some biases. For example, EnsMean delays RODs by about 20–30 days over SAS and 10–20 days over northern NAM while advancing them by 20–30 days over NAF and EAS. EnsMean shows less bias in simulated historical RCDs than RODs, with about 10–15 days of advance over NAF and NAM. Additionally, LRS is reasonably well represented. However, there are biases in the number of days, particularly in eastern NAF and SAS. Individual models generally struggle more with simulating RODs than RCDs, with higher percentage bias values for RODs across most regions. Except over EAS and AUS, future changes project a delay in RODs under the SSP2–4.5 and SSP5–8.5 scenarios in most monsoon regions, particularly under the 2.0°C GWL. The delays are more robust over regions like SAM, with models showing relatively low uncertainties. Conversely, under both scenarios, RCDs are projected to advance in some regions, such as NAM and AUS. The combined effects of changes in RODs and RCDs indicate a shortening of LRS over SAM and SAF, implying an intensification of dry conditions in a warming climate. Additionally, the study finds that total precipitation and the intensity of rainfall per day within the rainy season are projected to increase over most regions, particularly under the SSP5-8.5 scenario.

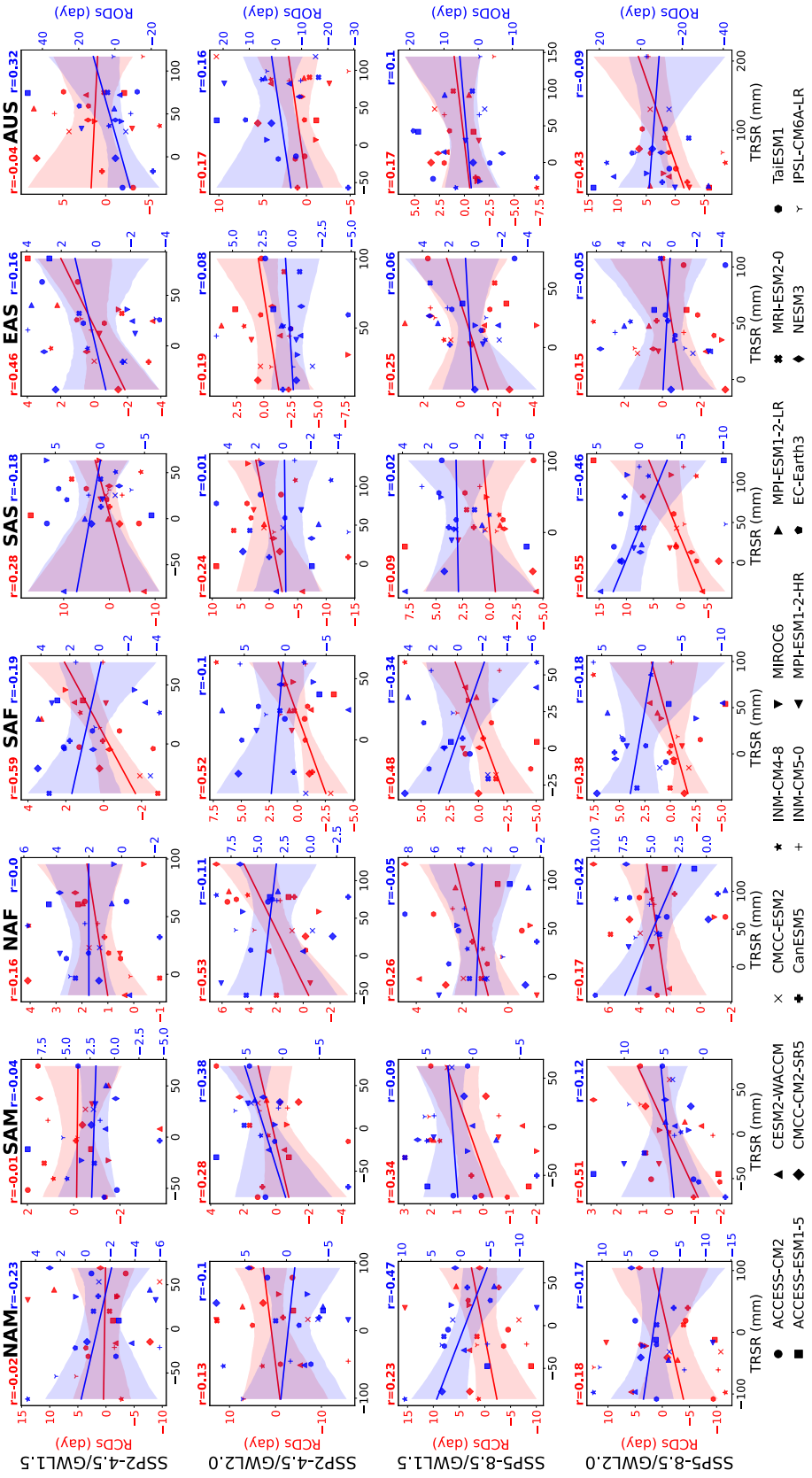

Fig. 9. Scatterplots and correlation coefficients showing the relationship between changes in total rainy season rainfall (TRSR; units: mm) and changes in rainfall onset dates (RODs; units: d) (blue) as well as rainfall cessation dates (RCDs; units: d) (red) under the SSP2-4.5 and SSP5-8.5 scenarios at various global warming levels (GWLs) relative to the period 1995–2014 for each monsoon region across the 16 CMIP6 ensemble members. Shading indicates 95% confidence intervals.

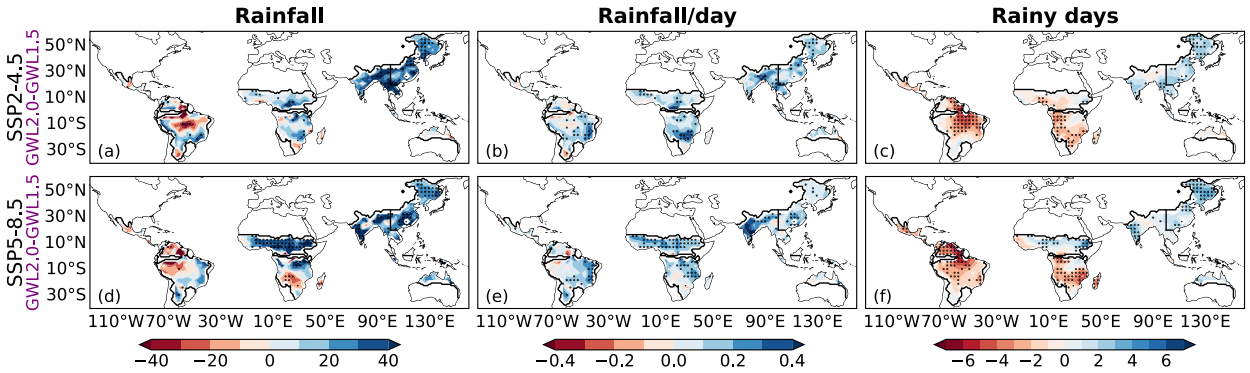

Fig. 10. Projected changes in total rainfall during the rainy season (units: mm), the daily rainfall rate (units: mm d^{-1}), and the number of rainy days (units: d) across GLM regions relative to the period 1995–2014 for the CMIP6 EnsMean models under the global warming level (GWL) of 2.0°C compared to that of 1.5°C for the (a–c) SSP2-4.5 and (d–f) SSP5-8.5 scenarios. Stippling marks areas where at least 70% of the models concur on the direction of change in EnsMean.

This increase is accompanied by a decrease in rainy days, suggesting a shift toward more intense but less frequent rainfall events. These findings underscore the importance of limiting global warming to below 2.0°C to mitigate adverse impacts on precipitation patterns and the length of the rainy season.

Changes in the timing of the rainy season can have significant implications for various sectors, particularly agriculture. For instance, the projected delays in the onset of the rainy season in SAM can disrupt planting schedules, reducing crop yields. Farmers rely on predictable rainfall patterns to time their planting, and any deviation can result in crops not reaching maturity before the end of the rainy season. Also, delayed onset affects water availability for irrigation and other uses. This can strain water resources, especially in regions already facing water scarcity. The timing of rainy season cessation also carries critical implications. For example, the projected early cessation over NAM and SAF can reduce the growing season, preventing crops from reaching full maturity and reducing yields. This is particularly detrimental for crops that require longer growing periods. Also, an early end to the rainy season can increase the risk of drought, affecting agriculture and water supply for domestic and industrial use. The overall length of the rainy season, determined by the onset and cessation dates, has profound implications. As projected in most GLM regions, a shortened rainy season can lead to insufficient crop water, reducing yields and potentially leading to food shortages. Also, changes in the length of the rainy season can alter the balance between flood and drought periods. However, in NAF, the projected increase in the TRSR, along with the RPRD, might mitigate drought risks but increase flooding incidents, damaging infrastructure, homes, and livelihoods, particularly in urban areas with poor drainage systems. Therefore, understanding the projected changes in rainfall characteristics is crucial for developing effective climate adaptation strategies. These include rainwater harvesting, improved irrigation techniques, and developing drought-resistant crop varieties.

Acknowledgements. We thank the World Climate Research Programme's Working Group on Coupled Modeling for managing the CMIP initiative, and express our gratitude to the climate modeling groups (as listed in Table S1) for their model outputs. We also appreciate the institution that provided the CPC observational data used in this research. Oluwafemi E. ADEYERI is supported by the Australian Research Council (Grant No. CE230100012).

Electronic supplementary material. Supplementary material is available in the online version of this article at https://doi.org/10.1007/s00376-025-4386-9.

REFERENCES

Adeyeri, O. E., W. Zhou, C. E. Ndehedehe, X. Wang, K. A. Ishola, and P. Laux, 2024: Minimizing uncertainties in climate projections and water budget reveals the vulnerability of freshwater to climate change. *One Earth*, **7**(1), 72–87, https://doi.org/10.1016/j.oneear.2023.12.013.

Akinsanola, A. A., and W. Zhou, 2019: Ensemble-based CMIP5 simulations of West African summer monsoon rainfall: Current climate and future changes. *Theor. Appl. Climatol.*, **136**(3–4), 1021–1031, https://doi.org/10.1007/s00704-018-2516-3.

Akinsanola, A. A., and W. Zhou, 2020: Understanding the variability of West African summer monsoon rainfall: Contrasting tropospheric features and monsoon index. *Atmosphere*, **11**(3), 309, https://doi.org/10.3390/atmos11030309.

Akinsanola, A. A., V. Ongoma, and G. J. Kooperman, 2021: Evaluation of CMIP6 models in simulating the statistics of

extreme precipitation over Eastern Africa. *Atmospheric Research*, **254**, 105509, https://doi.org/10.1016/j.atmosres.2021.105509.

Akinsanola, A. A., Z. M. Chen, G. J. Kooperman, and V. Bobde, 2024: Robust future intensification of winter precipitation over the United States. *Npj Climate and Atmospheric Science*, **7**(1), 212, https://doi.org/10.1038/s41612-024-00761-8.

Akinsanola, A. A., A. A. Adebiyi, V. Bobde, O. E. Adeyeri, A. T. Tamoffo, and D. K. Danso, 2025: Projected changes in African easterly wave activity due to climate change. *Communications Earth and Environment*, **6**(1), 2, https://doi.org/10.1038/s43247-024-01981-9.

Almazroui, M., F. Saeed, S. Saeed, M. N. Islam, M. Ismail, N. A. B. Klutse, and M. H. Siddiqui, 2020: Projected change in temperature and precipitation over Africa from CMIP6. *Earth Systems and Environment*, **4**(3), 455–475, https://doi.org/10.1007/s41748-020-00161-x.

Almazroui, M., and Coauthors, 2021: Assessment of CMIP6 performance and projected temperature and precipitation changes over South America. *Earth Systems and Environment*, **5**(2), 155–183, https://doi.org/10.1007/s41748-021-00233-6.

Amekudzi, L. K., E. I. Yamba, K. Preko, E. O. Asare, J. Aryee, M. Baidu, and S. N. A. Codjoe, 2015: Variabilities in rainfall onset, cessation and length of rainy season for the various agro-ecological zones of Ghana. *Climate*, **3**(2), 416–434, https://doi.org/10.3390/cli3020416.

Atiah, W. A., F. K. Muthoni, B. Kotu, F. Kizito, and L. K. Amekudzi, 2021: Trends of rainfall onset, cessation, and length of growing season in Northern Ghana: Comparing the rain gauge, satellite, and farmer's perceptions. *Atmosphere*, **12**(12), 1674, https://doi.org/10.3390/atmos12121674.

Ayugi, B., V. Dike, H. Ngoma, H. Babaousmail, R. Mumo, and V. Ongoma, 2021: Future changes in precipitation extremes over East Africa based on CMIP6 models. *Water*, **13**(17), 2358, https://doi.org/10.3390/w13172358.

Ayugi, B., and Coauthors, 2022: East African population exposure to precipitation extremes under 1.5 °C and 2.0 °C warming levels based on CMIP6 models. *Environmental Research Letters*, **17**(4), 044051, https://doi.org/10.1088/1748-9326/ac5d9d.

Bobde, V., A. A. Akinsanola, A. H. Folorunsho, A. A. Adebiyi, and O. E. Adeyeri, 2024: Projected regional changes in mean and extreme precipitation over Africa in CMIP6 models. *Environmental Research Letters*, **19**, 074009, https://doi.org/10.1088/1748-9326/ad545c.

Bombardi, R. J., and W. R. Boos, 2021: Explaining globally inhomogeneous future changes in monsoons using simple moist energy diagnostics. *J. Climate*, **34**(21), 8615–8634, https://doi.org/10.1175/jcli-d-20-1012.1.

Bombardi, R. J., J. L. Kinter, and O. W. Frauenfeld, 2019: A global gridded dataset of the characteristics of the rainy and dry seasons. *Bull. Amer. Meteor. Soc.*, **100**(7), 1315–1328, https://doi.org/10.1175/bams-d-18-0177.1.

Chakraborty, A., and P. Singhai, 2021: Asymmetric response of the Indian summer monsoon to positive and negative phases of major tropical climate patterns. *Scientific Reports*, **11**(1), 22561, https://doi.org/10.1038/s41598-021-01758-6.

Chang, M. Y., B. Liu, B. Wang, C. Martinez-Villalobos, G. Y. Ren, and T. J. Zhou, 2022: Understanding future increases in precipitation extremes in global land monsoon regions. *J. Climate*, **35**(6), 1839–1851, https://doi.org/10.1175/jcli-d-21-0409.1.

Chen, Z. M., T. J. Zhou, L. X. Zhang, X. L. Chen, W. X. Zhang, and J. Jiang, 2020: Global land monsoon precipitation changes in CMIP6 projections. *Geophys. Res. Lett.*, **47**, e2019GL086902, https://doi.org/10.1029/2019GL086902.

Cheng, Y. F., L. Wang, X. L. Chen, T. J. Zhou, and A. Turner, 2025: A shorter duration of the Indian summer monsoon in constrained projections. *Geophys. Res. Lett.*, **52**(1), e2024GL112848, https://doi.org/10.1029/2024gl112848.

Cheng, Y. E., L. Wang, X. L. Chen, T. J. Zhou, A. Turner, and L. J. Wang, 2024: Constrained projections indicate less delay in onset of summer monsoon over the Bay of Bengal and South China Sea. *Geophys. Res. Lett.*, **51**(21), e2024GL110994, https://doi.org/10.1029/2024gl110994.

Collini, E. A., E. H. Berbery, V. R. Barros, and M. E. Pyle, 2008: How does soil moisture influence the early stages of the South American monsoon? *J. Climate*, **21**(2), 195–213, https://doi.org/10.1175/2007jcli1846.1.

COP21, 2015: The Paris Agreement. United Nations Framework Convention on Climate Change (UNFCCC), Paris, France. [Available online from https://unfccc.int/process-and-meetings/the-paris-agreement/the-paris-agreement]

Daron, J., L. Burgin, T. Janes, R. G. Jones, and C. Jack, 2019: Climate process chains: Examples from southern Africa. *International Journal of Climatology*, **39**, 4784–4797, https://doi.org/10.1002/joc.6106.

Das, S., M. Kamruzzaman, and A. R. M. T. Islam, 2022: Assessment of characteristic changes of regional estimation of extreme rainfall under climate change: A case study in a tropical monsoon region with the climate projections from CMIP6 model. *J. Hydrol.*, **610**, 128002, https://doi.org/10.1016/j.jhydrol.2022.128002.

Dash, S. K., R. K. Jenamani, S. R. Kalsi, and S. K. Panda, 2007: Some evidence of climate change in twentieth-century India. *Climatic Change*, **85**(3–4), 299–321, https://doi.org/10.1007/s10584-007-9305-9.

Deng, K. Q., S. Yang, M. Ting, Y. H. Tan, and S. He, 2018: Global monsoon precipitation: Trends, leading modes, and associated drought and heat wave in the Northern Hemisphere. *J. Climate*, **31**, 6947–6966, https://doi.org/10.1175/JCLI-D-17-0569.1.

Donat, M. G., A. L. Lowry, L. V. Alexander, P. A. O'Gorman, and N. Maher, 2016: More extreme precipitation in the world's dry and wet regions. *Nature Climate Change*, **6**(5), 508–513, https://doi.org/10.1038/nclimate2941.

Dosio, A., and Coauthors, 2021: Projected future daily characteristics of African precipitation based on global (CMIP5, CMIP6) and regional (CORDEX, CORDEX-CORE) climate models. *Climate Dyn.*, **57**(11–12), 3135–3158, https://doi.org/10.1007/s00382-021-05859-w.

Dunning, C. M., E. Black, and R. P. Allan, 2018: Later wet seasons with more intense rainfall over Africa under future climate change. *J. Climate*, **31**(23), 9719–9738, https://doi.org/10.1175/jcli-d-18-0102.1.

Dwyer, J. G., M. Biasutti, and A. H. Sobel, 2014: The effect of greenhouse gas–induced changes in SST on the annual cycle of zonal mean tropical precipitation. *J. Climate*, **27**(12), 4544–4565, https://doi.org/10.1175/jcli-d-13-00216.1.

Eyring, V., S. Bony, G. A. Meehl, C. A. Senior, B. Stevens, R. J. Stouffer, and K. E. Taylor, 2016: Overview of the Coupled Model Intercomparison Project Phase 6 (CMIP6) experimental design and organization. *Geoscientific Model Develop-*

ment, **9**(5), 1937–1958, https://doi.org/10.5194/gmd-9-1937-2016.

Faye, A., and A. A. Akinsanola, 2022: Evaluation of extreme precipitation indices over West Africa in CMIP6 models. *Climate Dyn.*, **58**(3–4), 925–939, https://doi.org/10.1007/s00382-021-05942-2.

Gadgil, S., and S. Gadgil, 2006: The Indian monsoon, GDP and agriculture. *Economic and Political Weekly*, **41**, 4887–4895.

Ha, K.-J., S. Moon, A. Timmermann, and D. Kim, 2020: Future changes of summer monsoon characteristics and evaporative demand over Asia in CMIP6 simulations. *Geophys. Res. Lett.*, **47**, e2020GL087492, https://doi.org/10.1029/2020GL087492.

Hariadi, M. H., and Coauthors, 2022: Evaluation of onset, cessation and seasonal precipitation of the Southeast Asia rainy season in CMIP5 regional climate models and HighResMIP global climate models. *International Journal of Climatology*, **42**(5), 3007–3024, https://doi.org/10.1002/joc.7404.

Hauser, M., F. Engelbrecht, and E. M. Fischer, 2022: Transient global warming levels for CMIP5 and CMIP6, https://doi.org/10.5281/zenodo.3591806.

Hodnebrog, Ø., B. M. Steensen, L. Marelle, K. Alterskjær, S. B. Dalsøren, and G. Myhre, 2022: Understanding model diversity in future precipitation projections for South America. *Climate Dyn.*, **58**(5–6), 1329–1347, https://doi.org/10.1007/s00382-021-05964-w.

Intergovernmental Panel on Climate Change (IPCC), 2021: *Climate Change 2021: The Physical Science Basis. Contribution of Working Group I to the Sixth Assessment Report of the Intergovernmental Panel on Climate Change*. Cambridge University Press.

Jin, C. H., B. Wang, and J. Liu, 2020: Future changes and controlling factors of the eight regional monsoons projected by CMIP6 models. *J. Climate*, **33**(21), 9307–9326, https://doi.org/10.1175/jcli-d-20-0236.1.

Jones, C., and L. M. V. Carvalho, 2013: Climate change in the South American monsoon system: Present climate and CMIP5 projections. *J. Climate*, **26**(17), 6660–6678, https://doi.org/10.1175/JCLI-D-12-00412.1.

Khadka, D., M. S. Babel, A. A. Abatan, and M. Collins, 2022: An evaluation of CMIP5 and CMIP6 climate models in simulating summer rainfall in the Southeast Asian monsoon domain. *International Journal of Climatology*, **42**(2), 1181–1202, https://doi.org/10.1002/joc.7296.

Kitoh, A., H. Endo, K. Krishna Kumar, I. F. A. Cavalcanti, P. Goswami, and T. J. Zhou, 2013: Monsoons in a changing world: A regional perspective in a global context. *J. Geophys. Res.: Atmos.*, **118**(8), 3053–3065, https://doi.org/10.1002/jgrd.50258.

Kumi, N., and B. J. Abiodun, 2018: Corrigendum: Potential impacts of 1.5 °C and 2 °C global warming on rainfall onset, cessation and length of rainy season in West Africa (2018 *Environ. Res. Lett.* **13** 055009). *Environmental Research Letters*, **13**(8), 089502, https://doi.org/10.1088/1748-9326/aad5c6.

Lee, J.-Y., and B. Wang, 2014: Future change of global monsoon in the CMIP5. *Climate Dyn.*, **42**(1–2), 101–119, https://doi.org/10.1007/s00382-012-1564-0.

Lehmann, J., D. Coumou, and K. Frieler, 2015: Increased record-breaking precipitation events under global warming. *Climatic Change*, **132**(4), 501–515, https://doi.org/10.1007/s10584-015-1434-y.

Liebmann, B., and J. Marengo, 2001: Interannual variability of the rainy season and rainfall in the Brazilian Amazon basin. *J. Climate*, **14**(22), 4308–4318, https://doi.org/10.1175/1520-0442(2001)014<4308:ivotrs>2.0.co;2.

Liu, F., B. Wang, Y. Ouyang, H. Wang, S. B. Qiao, G. S. Chen, and W. J. Dong, 2022: Intraseasonal variability of global land monsoon precipitation and its recent trend. *Npj Climate and Atmospheric Science*, **5**(1), 30, https://doi.org/10.1038/s41612-022-00253-7.

Majdi, F., S. A. Hosseini, A. Karbalaee, M. Kaseri, and S. Marjanian, 2022: Future projection of precipitation and temperature changes in the Middle East and North Africa (MENA) region based on CMIP6. *Theor. Appl. Climatol.*, **147**(3–4), 1249–1262, https://doi.org/10.1007/s00704-021-03916-2.

Menon, A., A. Levermann, J. Schewe, J. Lehmann, and K. Frieler, 2013: Consistent increase in Indian monsoon rainfall and its variability across CMIP-5 models. *Earth System Dynamics*, **4**(2), 287–300, https://doi.org/10.5194/esd-4-287-2013.

Mishra, A., and S. C. Liu, 2014: Changes in precipitation pattern and risk of drought over India in the context of global warming. *J. Geophys. Res.: Atmos.*, **119**(13), 7833–7841, https://doi.org/10.1002/2014jd021471.

Moon, S., and K.-J. Ha, 2020: Future changes in monsoon duration and precipitation using CMIP6. *npj Climate and Atmospheric Science*, **3**, 45, https://doi.org/10.1038/s41612-020-00151-w.

Mugalavai, E. M., E. C. Kipkorir, D. Raes, and M. S. Rao, 2008: Analysis of rainfall onset, cessation and length of growing season for western Kenya. *Agricultural and Forest Meteorology*, **148**(6–7), 1123–1135, https://doi.org/10.1016/j.agrformet.2008.02.013.

Mwangi, E., D. MacLeod, D. Kniveton, and M. C. Todd, 2024: Variability of rainy season onsets over East Africa. *International Journal of Climatology*, **44**, 3357–3379, https://doi.org/10.1002/joc.8528.

Ni, Y., and P. C. Hsu, 2018: Inter-annual variability of global monsoon precipitation in present-day and future warming scenarios based on 33 Coupled Model Intercomparison Project Phase 5 models. *International Journal of Climatology*, **38**(13), 4875–4890, https://doi.org/10.1002/joc.5704.

Nicholson, S. E., 2018: The ITCZ and the seasonal cycle over equatorial Africa. *Bull. Amer. Meteor. Soc.*, **99**, 337–348, https://doi.org/10.1175/BAMS-D-16-0287.1.

Omay, P. O., N. J. Muthama, C. Oludhe, J. M. Kinama, G. Artan, and Z. Atheru, 2023: Changes and variability in rainfall onset, cessation, and length of rainy season in the IGAD region of Eastern Africa. *Theor. Appl. Climatol.*, **152**(1–2), 871–893, https://doi.org/10.1007/s00704-023-04433-0.

Omondi, P. A., and Coauthors, 2014: Changes in temperature and precipitation extremes over the Greater Horn of Africa region from 1961 to 2010. *International Journal of Climatology*, **34**(4), 1262–1277, https://doi.org/10.1002/joc.3763.

Omotosho, J. B., A. A. Balogun, and K. Ogunjobi, 2000: Predicting monthly and seasonal rainfall, onset and cessation of the rainy season in West Africa using only surface data. *International Journal of Climatology*, **20**, 865–880, https://doi.org/10.1002/1097-0088(20000630)20:8<865::AID-JOC505>3.0.CO;2-R.

O'Neill, B. C., and Coauthors, 2017: The roads ahead: Narratives for shared socioeconomic pathways describing world futures in the 21st century. *Global Environmental Change*, **42**, 169–180, https://doi.org/10.1016/j.gloenvcha.2015.01.004.

Piao, J., W. Chen, J. S. Kim, W. Zhou, S. F. Chen, P. Hu, and X. Q. Lan, 2023: Future changes in rainy season characteristics over East China under continuous warming. *Climatic Change*, **176**(9), 120, https://doi.org/10.1007/s10584-023-03598-x.

Preethi, B., M. Mujumdar, R. H. Kripalani, A. Prabhu, and R. Krishnan, 2017: Recent trends and tele-connections among South and East Asian summer monsoons in a warming environment. *Climate Dyn.*, **48**(7–8), 2489–2505, https://doi.org/10.1007/s00382-016-3218-0.

Sabeerali, C. T., and R. S. Ajayamohan, 2018: On the shortening of Indian summer monsoon season in a warming scenario. *Climate Dyn.*, **50**(5–6), 1609–1624, https://doi.org/10.1007/s00382-017-3709-7.

Seager, R., N. Naik, and G. A. Vecchi, 2010: Thermodynamic and dynamic mechanisms for large-scale changes in the hydrological cycle in response to global warming. *J. Climate*, **23**(17), 4651–4668, https://doi.org/10.1175/2010jcli3655.1.

Seth, A., A. Giannini, M. Rojas, S. A. Rauscher, S. Bordoni, D. Singh, and S. J. Camargo, 2019: Monsoon responses to climate changes-Connecting past, present and future. *Current Climate Change Reports*, **5**, 63–79, https://doi.org/10.1007/s40641-019-00125-y.

Sharmila, S., S. Joseph, A. K. Sahai, S. Abhilash, and R. Chattopadhyay, 2015: Future projection of Indian summer monsoon variability under climate change scenario: An assessment from CMIP5 climate models. *Global and Planetary Change*, **124**, 62–78, https://doi.org/10.1016/j.gloplacha.2014.11.004.

Singhai, P., A. Chakraborty, K. Rajendran, and S. Surendran, 2023: Why is the Indian summer monsoon in CFSv2 hypersensitive to moisture exchange with the Pacific Ocean? *Climate Dyn.*, **61**(9), 4515–4531, https://doi.org/10.1007/s00382-023-06815-6.

Sylla, M. B., I. Diallo, and J. S. Pal, 2013: West African monsoon in state-of-the-science regional climate models. *Climate Variability-Regional and Thematic Patterns*, A. Tarhule, Ed., InTech, https://doi.org/10.5772/55140.

Sylla, M. B., P. M. Nikiema, P. Gibba, I. Kebe, and N. A. B. Klutse, 2016: Climate change over West Africa: Recent trends and future projections. *Adaptation to Climate Change and Variability in Rural West Africa*, J. A. Yaro and J. Hesselberg, Eds., Springer, 25–40, https://doi.org/10.1007/978-3-319-31499-0_3.

Taguela, T. N., A. A. Akinsanola, V. Bobde, I. Raji, O. E. Adeyeri, and A. A. Adebiyi, 2025: Precipitation distribution over Africa: Observations and modeling. *Aerosols and Precipitation over Africa*, A. A. Akinsanola and A. A. Adebiyi, Eds., Elsevier, 121–146, https://doi.org/10.1016/b978-0-44-314050-1.00009-8.

Taguela, T. N., and Coauthors, 2020: CORDEX Multi-RCM Hindcast over Central Africa: Evaluation within observational uncertainty. *J. Geophys. Res.: Atmos.*, **125**(5), e2019JD031607, https://doi.org/10.1029/2019JD031607.

Turner, A. G., and H. Annamalai, 2012: Climate change and the South Asian summer monsoon. *Nature Climate Change*, **2**(8), 587–595, https://doi.org/10.1038/nclimate1495.

Vera, C., G. Silvestri, B. Liebmann, and P. González, 2006: Climate change scenarios for seasonal precipitation in South America from IPCC-AR4 models. *Geophys. Res. Lett.*, **33**, L13707, https://doi.org/10.1029/2006GL025759.

Wainwright, C. M., E. Black, and R. P. Allan, 2021: Future changes in wet and dry season characteristics in CMIP5 and CMIP6 simulations. *Journal of Hydrometeorology*, **22**, 2339–2357, https://doi.org/10.1175/jhm-d-21-0017.1.

Wang, B., and Q. H. Ding, 2008: Global monsoon: Dominant mode of annual variation in the tropics. *Dyn. Atmos. Oceans*, **44**(3–4), 165–183, https://doi.org/10.1016/j.dynatmoce.2007.05.002.

Wang, B., C. H. Jin, and J. Liu, 2020: Understanding future change of global monsoons projected by CMIP6 models. *J. Climate*, **33**(15), 6471–6489, https://doi.org/10.1175/jcli-d-19-0993.1.

Wang, B., J. Liu, H.-J. Kim, P. J. Webster, and S.-Y. Yim, 2012: Recent change of the global monsoon precipitation (1979–2008). *Climate Dyn.*, **39**(5), 1123–1135, https://doi.org/10.1007/s00382-011-1266-z.

Wang, L., Y. F. Cheng, X. L. Chen, and T. J. Zhou, 2024: Projected changes in the onset of the summer monsoon over the South Asian marginal seas modulated by intraseasonal oscillation. *J. Climate*, **37**(3), 821–835, https://doi.org/10.1175/jcli-d-23-0257.1.

Wang, P. X., B. Wang, H. Cheng, J. Fasullo, Z. T. Guo, T. Kiefer, and Z. Y. Liu, 2017b: The global monsoon across time scales: Mechanisms and outstanding issues. *Earth-Science Reviews*, **174**, 84–121, https://doi.org/10.1016/j.earscirev.2017.07.006.

Xie, P. P., M. Chen, and W. Shi, 2010: CPC Unified gauge-based analysis of global daily precipitation. *24th Conf. on Hydrology*, Atlanta, GA, Amer. Meteor. Soc., 2.3A.

Yao, J. Q., Y. N. Chen, J. Chen, Y. Zhao, D. Tuoliewubieke, J. G. Li, L. M. Yang, and W. Y. Mao, 2021: Intensification of extreme precipitation in arid Central Asia. *J. Hydrol.*, **598**, 125760, https://doi.org/10.1016/j.jhydrol.2020.125760.

Yim, S. Y., B. Wang, J. Liu, and Z. W. Wu, 2014: A comparison of regional monsoon variability using monsoon indices. *Climate Dyn.*, **43**(5–6), 1423–1437, https://doi.org/10.1007/s00382-013-1956-9.

Zhang, W. J., H. Y. Li, M. F. Stuecker, F. F. Jin, and A. G. Turner, 2016: A new understanding of El Niño's impact over East Asia: Dominance of the ENSO combination mode. *J. Climate*, **29**(12), 4347–4359, https://doi.org/10.1175/JCLI-D-15-0104.1.

Zhang, W. X., and T. J. Zhou, 2019: Significant increases in extreme precipitation and the associations with global warming over the global land monsoon regions. *J. Climate*, **32**(24), 8465–8488, https://doi.org/10.1175/JCLI-D-18-0662.1.

Zhang, W. X., and T. J. Zhou, 2020: Increasing impacts from extreme precipitation on population over China with global warming. *Science Bulletin*, **65**(3), 243–252, https://doi.org/10.1016/j.scib.2019.12.002.

Zhang, X. B., L. Alexander, G. C. Hegerl, P. Jones, A. K. Tank, T. C. Peterson, B. Trewin, and F. W. Zwiers, 2011: Indices for monitoring changes in extremes based on daily temperature and precipitation data. *WIREs Climate Change*, **2**(6), 851–870, https://doi.org/10.1002/wcc.147.

Zhou, T. J., J. W. Lu, W. X. Zhang, and Z. M. Chen, 2020: The sources of uncertainty in the projection of global land monsoon precipitation. *Geophys. Res. Lett.*, **47**, e2020GL088415, https://doi.org/10.1029/2020GL088415.